

## Recovery of rare earths and lithium from rare earth molten salt electrolytic slag by lime transformation, co-leaching and stepwise precipitation

Xinglan Li <sup>1,2,3</sup>, Peidi Luo <sup>4</sup>, Zishuai Liu <sup>1,2,3</sup>, Xuekun Tang <sup>1,2,3</sup>, Baqun Zhang <sup>1,2,3</sup>, Jiangfeng Guo <sup>1,2</sup>

<sup>1</sup> Faculty of Resource and Environmental Engineering, Jiangxi University of Science and Technology, Ganzhou 341000, China

<sup>2</sup> Key Laboratory of Testing and Tracing of Rare Earth Products for State Market Regulation, Jiangxi University of Science and Technology, Ganzhou 341000, China

<sup>3</sup> Yichun Lithium New Energy Industry Research Institute, Jiangxi University of Science and Technology, Yichun 336000, China

<sup>4</sup> School of Energy Science and Engineering, Harbin Institute of Technology, Harbin 150006, China

Corresponding authors: liuzishuai87@126.com (Zishuai Liu), txk0797@126.com (Xuekun Tang)

**Abstract:** The rare earth molten salt electrolytic slag (REMSES) has recently attracted significant attention due to its potential environmental hazards and high content of rare earths and lithium, leading to a surge in recycling efforts. In this study, we propose and demonstrate a novel and straightforward process for the simultaneous extraction of rare earths and lithium from REMSES through lime transformation and sulfuric acid leaching at low temperatures. Firstly, during the lime transformation process, REMSES is converted into hydroxides that can be easily dissolved in acids. Secondly, REEs and Li present in the slag are co-extracted using a conditional sulfuric acid leaching method, resulting in 95.72% REEs leaching efficiency and 99.41% Li leaching efficiency under optimal conditions. Finally, REEs and Li in the solution are precipitated using oxalic acid and trisodium phosphate with precipitation efficiencies of 99.02% for REEs and 94.85% for Li respectively. This innovative process enables the conversion of REEs and lithium from REMSES into high-purity products (a mixture of REOs with 99.31% purity;  $\text{Li}_3\text{PO}_4$  with 98.93% purity), thereby facilitating their valuable utilization.

**Keywords:** rare earth molten salt electrolytic slag, lime transforming, leaching, lithium, recovery

### 1. Introduction

The rare earth elements (REEs) are a group of elements that include scandium, yttrium, and 15 lanthanides. Due to their exceptional physical and chemical properties, these elements are extensively utilized in various high-tech fields as significant strategic resources, such as permanent magnet materials, optoelectronic materials, special alloy materials, etc (Su et al., 2020; Georgios et al., 2015; Ji et al., 2022). The molten salt electrolysis process is widely employed for the preparation of different reactive metal elements and their alloys due to its advantages of high product purity, low cost, and easy implementation of continuous operation. Currently, rare earth metals and their alloys are primarily produced through the molten salt electrolysis process under fluoride system ( $\text{REF}_3\text{-LiF-RE}_2\text{O}_3$ ) or chloride system ( $\text{RECl}_3$ ) (Sun et al., 2022; Yang et al., 2019; Feng et al., 2023; Chen et al., 2023; Gu et al., 2017; Chen et al., 2021; Lai et al., 2023). Presently, considering the benefits of a more stable electrolyte composition with better hydrolysis resistance, higher current efficiency and rare earth yield along with being more environmentally friendly; the fluoride molten salts system ( $\text{REF}_3\text{-LiF-RE}_2\text{O}_3$ ) is more commonly used in rare earth metal molten-salt electrolytic processes compared to the  $\text{RECl}_3$  system (Yang et al., 2023; Liu et al., 2023; Liang et al., 2018; Prince et al., 2021). During the rare earth metal molten salt electrolytic processes, a substantial amount of non-rare earth impurities accumulate in the

rare earth molten salt during operations like rare earth metal discharge, anode replacement regular furnace cleaning and dismantling, making it challenging to avoid generating waste REMSES (Tian et al., 2021; Tong et al., 2022). At present global production of rare earth oxides (REOs) has reached 126000 tons per year with approximately 5-8% lost in REMSES (Dushyantha et al., 2020; Cai et al., 2018). Therefore, the recovery of rare earth and lithium from REMSES holds significant scientific and academic importance.

Electrolytic slags have recently attracted significant attention owing to their potential environmental hazards and their content of high value elements (REEs and lithium), driving recycling reaches mushrooming. A multitude of extraction systems have been proposed for the recycling of electrolytic slags. An experimental study of rare earth recovery from the fluorinated rare earth molten-salt electrolytic slag by sodium carbonate roasting-hydrochloric acid leaching was carried out by Wu et al (2023), based on the principle that rare earth fluoride can be converted into rare earth hydroxide when heated under alkaline conditions. This method involves dissolving the rare earth hydroxide with sodium hydroxide, thereby converting acid-insoluble rare earth fluoride into soluble rare earth hydroxide under atmospheric pressure. A clean process for recycling rare-earth molten salt electrolytic slag via fluorine fixation roasting using calcium oxide and calcium chloride and hydrometallurgical hydrochloric acid leaching, as investigated by Xing et al (2023), utilizes calcium oxide and calcium chloride as the solid reagent for the conversion of rare earth fluorides into rare earth hydroxides through roasting. The recovery of rare earths from REMSES by using borax roasting followed by hydrochloric acid leaching was conducted by Yang et al (2020). In this method, The rare earth fluorides react with borax to form rare earth oxides in the roasting step, they promoted the rare earth recovery by increasing the roasting temperature, reaction time and borax dosage. The methods of selective sulfation and nitration were explored by Wang (2021) and Hu (2021). The researchers utilized a selective nitration method to completely convert powdered samples into a mixture of nitrates or sulfates, followed by appropriate selective roast-water leaching treatments. Consequently, the extraction efficiency for the REEs and lithium surpassed 98%. In summary, the routes can be classified as acid roasting, alkaline roasting, or salt roasting, all of which involve a high-temperature roasting process to achieve efficient recovery of target metals. The primary focus lies on REEs, with less emphasis placed on lithium. However, there are drawbacks such as lengthy processing time, substantial equipment demand, stringent equipment specifications and energy consumption, as well as the absence of lithium recycling. Therefore, it is imperative to develop a cost-effective and low-temperature process for extracting both REEs and lithium from REMSES with high recovery rates.

Currently, the primary techniques employed for lithium recovery from solution encompass solvent extraction and chemical precipitation, encompassing both the lithium carbonate and lithium phosphate pathways. As a common route for lithium extraction from salt lakes, the tributyl phosphate (TBP)-FeCl<sub>3</sub>-kerosene system has low lithium extraction efficiency for the instability of FeCl<sub>4</sub><sup>-</sup> and TBP (Duan et al., 2024). The precipitation of lithium carbonate from lithium sulfate media by the addition of sodium carbonate was reported by Liu (2021) in the context of the lithium carbonate route. Consequently, the lithium recovery efficiency was suboptimal and attaining the desired product purity proved challenging. The low solubility product constant of lithium phosphate enables the utilization of phosphate for enhancing the concentration and precipitation of lithium from dilute solutions. Wu (2023) proposed a straightforward and efficient approach for extracting lithium from low-lithium resources through the processes of mixed acid leaching and lithium phosphate precipitation from bauxite mine tailings. Mulwanda (2023) performed the lithium extraction process from lepidolite concentrate through roasting with NaHSO<sub>4</sub>, followed by water leaching and phosphoric acid precipitation, resulting in a lithium recovery rate of approximately 93%. The solubility product constant ( $K_{sp}=2.37\times 10^{-4}$ ) of lithium phosphate is lower than that of lithium carbonate ( $K_{sp}=1.7\times 10^{-3}$ ) (Wang et al., 2018), thus enabling the precipitation of lithium from dilute solutions through the process of lithium phosphate precipitation.

A novel approach was proposed and demonstrated in the current research, aiming to achieve the efficient and cost-effective extraction of both REEs and Li. Firstly, through lime transformation, REMSES was converted into hydroxides that could be readily dissolved in acids. Secondly, a conditional sulfuric acid leaching process was employed to extract REEs and Li from the slag, resulting in their successful recovery. Finally, oxalic acid and trisodium phosphate were utilized to precipitate REEs and Li from

the solution respectively. This innovative and straightforward approach enables the conversion of REEs and lithium present in REMSES into high-purity products, thereby facilitating their valuable utilization. Consequently, it offers a promising method for the comprehensive recovery of rare earth elements and lithium from REMSES.

## 2. Experimental

### 2.1. Experimental operations

All operations were carried out on a platform equipped with a fume hood. Leaching and stepwise precipitation were conducted in PTFE beakers fitted with a magnetic stirring bar. After the materials were added to the PTFE beakers, the beakers were sealed by films with small holes.

#### 2.1.1. Lime transforming

The rare earth molten salt electrolytic slag was mixed with a certain mass of CaO together with a certain volume (L/S ratio 1) of deionized water at a given temperature at a speed of 300 r/min in the PTFE beakers for a certain time.

#### 2.1.2. Leaching

After the lime transforming of the mixture was completed, sulfuric acid is added to a PTFE beaker containing the mixture and stirred at a given temperature at a speed of 300 r/min for a certain time. After the reaction was completed, the product was filtered and separated into liquids and solids. The leachate was analyzed, and the leaching residue was characterized. The leaching efficiencies of the REEs and Li were calculated as follows:

$$E_1 = \frac{CV}{gm} \times 100\% \quad (1)$$

where  $E_1$  is the leaching efficiency of metal elements, %;  $C$  is the concentration of metal elements in the leachate, g/L;  $V$  is the leachate volume, L;  $g$  is the grade of metal in the slag, %; and  $m$  is the mass of the slag.

#### 2.1.3. REEs precipitation

After removing most solid in leachate, a solution at pH 0.2 with 66.16 g/L REEs(calculated in TREO) and 4.05 g/L Li was finally obtained. With heated at certain temperature and stirred at 300 r/min, the leachate was added to a beaker, and a certain amount of oxalic acid was slowly added to the beaker (Liu et al., 2022). After the reaction was completed, the solid and liquid were filtered to obtain the rare earth oxalates and solution after precipitation of REEs. The rare earth oxalates were characterized, and the solution after precipitation of REEs was analyzed. The precipitation efficiency of the REEs was calculated as follows:

$$E_2 = \frac{c_1V_1 - c_2V_2}{c_1V_1} \times 100\% \quad (2)$$

where  $E_2$  is the precipitation efficiency of the metal elements, %;  $C_1$  is the concentration of metal elements in the leachate, g/L;  $V_1$  is the leachate volume, L;  $C_2$  is the concentration of metal elements in the solution after precipitation of REEs, g/L; and  $V_2$  is the volume of the precipitated REEs solution after precipitation of REEs, L.

#### 2.1.4. Li precipitation

The solution after precipitation of REEs was treated with certain amount of hydrogen peroxide solution to pH 8 and then saturated sodium hydroxide solution to pH 11 in preparation for removal of most of the impurities(Fe, Al, Ca, Mg) in the solution, with heated to 90°C and stirred at 300 r/min, the solution after precipitation of REEs was added to a beaker, and a certain amount (a mole ratio  $\text{Na}_3\text{PO}_4/\text{Li}$  of 1.1) trisodium phosphate was slowly added to the beaker (Wu et al., 2023). After the reaction was complete, filtration was carried out, and the white precipitate and solution after Li precipitation were obtained.

The white precipitate was characterized, and the solution after Li precipitation was analyzed. The precipitation efficiency of Li was calculated as follows:

$$E_3 = \frac{C_2V_2 - C_3V_3}{C_2V_2} \times 100\% \quad (3)$$

where  $E_3$  is the precipitation efficiency of Li, %;  $C_3$  is the Li concentration in the precipitated Li wastewater, g/L; and  $V_3$  is the precipitated Li wastewater volume, L.

## 2.2. Characterization and analytical methods

After being ground to 200 mesh, the molten salt electrolytic slag, lime transformed slag, leaching residue, and condensate were analyzed by X-ray diffraction (Ultima IV, Rigaku, Japan). The morphology of slags and products were characterized by scanning electron microscopy (MLA650F, FEI Company, USA). The elemental analysis of slag and solution was analyzed by inductively coupled plasma optical emission spectrometer (Optima 8000, PerkinElmer, USA) and atomic absorption spectroscopy (PinAAcle 900F, PerkinElmer, USA). The elemental analysis of rare earth and other elements was tested using the National standard testing method of China (GB/T 14635-2020: Rare earth metals and their compounds – Determination of total rare earth content) (Inspection and Quarantine of the People's Republic of China, 2020).

## 3. Results and discussion

### 3.1. Materials and analysis

The REMSES was obtained from a rare earth resources recovery company in Ganzhou, Jiangxi Province. To increase leaching efficiency and accelerate the reaction rate, the slag was crushed and ground into particles that could pass through a 200 mesh sieve. The chemical composition and rare earth distribution in the slag are listed in Table 1 and Table 2. The analysis shows that the slag contains 28.07% TREO (mainly Cerium and Gadolinium, calculated by oxides), 13.00% Si, 14.38% F, 6.20% Mn, 4.95% Fe, 1.64% Li. As the XRD pattern analysis shown in Fig.1, the majority crystalline phases of the slag were  $CeF_3$  (Ref.00-049-1058),  $LaF_3$  (Ref.00-049-1058),  $NdF_3$  (Ref.00-049-1058),  $CeOF$  (Ref.00-021-0183),  $LaOF$  (Ref.01-089-5166), together with  $C$  (Ref.01-089-8487),  $LiF$  (Ref.00-004-0857),  $LiGdSiO_4$  (Ref. 00-048-0009) as minor phases.

Table 1. Chemical composition of the REMSES (wt. %)

TREO	F	Si	Mn	Fe	Li	Al	Mg
28.07	14.38	13.00	6.20	4.95	1.64	1.62	1.54

Table 2. Rare earth distribution of the REMSES (wt. %).

$La_2O_3$	$CeO_2$	$Pr_6O_{11}$	$Nd_2O_3$	$Sm_2O_3$	$Gd_2O_3$	$Ho_2O_3$	Others
10.1	48.54	3.09	13.17	0.51	23.90	0.50	0.19

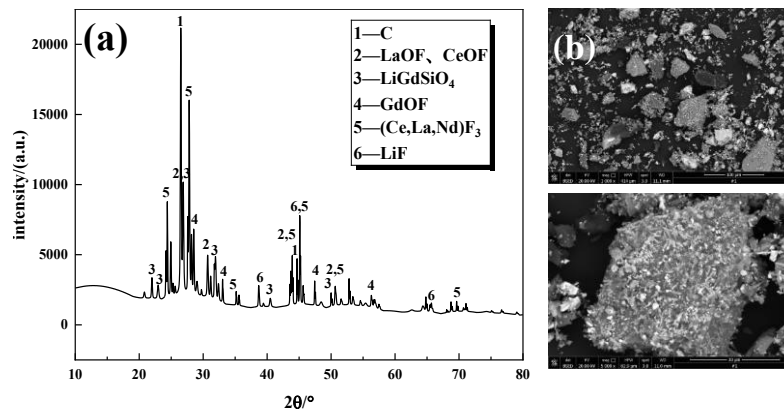


Fig. 1. XRD (a) and SEM (b) of the rare earth molten salt electrolytic slag

### 3.2. Effect of lime transformation on rare earth and lithium leaching

The rare earth elements (REEs) in REMSES predominantly exist as rare earth fluorides, which pose challenges for direct leaching through conventional acid leaching methods due to their low solubility product constants and acidic system properties (Chen et al., 2023). The solubility product constant of rare earth hydroxides is comparatively lower than that of rare earth fluorides; however, their stability in acidic systems is relatively weaker, making them susceptible to acid leaching. Therefore, it can be considered advantageous to convert the rare earth fluorides present in REMSES into hydroxides under strong alkali conditions and subsequently subject them to acid leaching. Table 3 lists the solubility product constants of fluoride and hydroxide for some REEs (Wang et al., 2018; Li et al., 2009).

Table 3. Solubility product constant of some fluorides and hydroxides.

Compounds	LaF <sub>3</sub>	CeF <sub>3</sub>	PrF <sub>3</sub>	NdF <sub>3</sub>	GdF <sub>3</sub>	CaF <sub>2</sub>
K <sub>sp</sub>	7.9×10 <sup>-18</sup>	7.9×10 <sup>-18</sup>	1.0×10 <sup>-17</sup>	7.9×10 <sup>-18</sup>	5.0×10 <sup>-16</sup>	5.2×10 <sup>-9</sup>
Compounds	La(OH) <sub>3</sub>	Ce(OH) <sub>3</sub>	Pr(OH) <sub>3</sub>	Nd(OH) <sub>3</sub>	Gd(OH) <sub>3</sub>	Ca(OH) <sub>2</sub>
K <sub>sp</sub>	1.0×10 <sup>-19</sup>	1.5×10 <sup>-20</sup>	2.7×10 <sup>-20</sup>	1.9×10 <sup>-21</sup>	1.0×10 <sup>-19</sup>	5.5×10 <sup>-6</sup>

The HSC Chemistry software (Outokumpu Technology Company, 2012) was used to calculate the thermodynamic data for the relevant reactions during the lime transforming of the REMSES. The relationship between temperature T and the reaction Gibbs free energy change ( $\Delta G$ ) is shown in Table 4 and Fig. 2. The results indicate that the  $\Delta G$  values for all reactions are negative within the specified temperature range, suggesting their spontaneous nature in this given temperature range.

Table 4. Gibbs free energy of reactions during the lime transforming of REMSES (20-100°C).

No.	Reaction	$\Delta_r G \sim T$ (kJ/mol)
1	$LaF_3 + 1.5Ca(OH)_2 = La(OH)_3 + 1.5CaF_2$	0.0116T-72.541
2	$CeF_3 + 1.5Ca(OH)_2 = Ce(OH)_3 + 1.5CaF_2$	0.0182T-90.862
3	$PrF_3 + 1.5Ca(OH)_2 = Pr(OH)_3 + 1.5CaF_2$	0.0127T-84.634
4	$NdF_3 + 1.5Ca(OH)_2 = Nd(OH)_3 + 1.5CaF_2$	0.0137T-95.656
5	$GdF_3 + 1.5Ca(OH)_2 = Gd(OH)_3 + 1.5CaF_2$	0.011T-69.628
6	$2LiF + Ca(OH)_2 = 2LiOH(a) + CaF_2$	-0.0938T-36.744

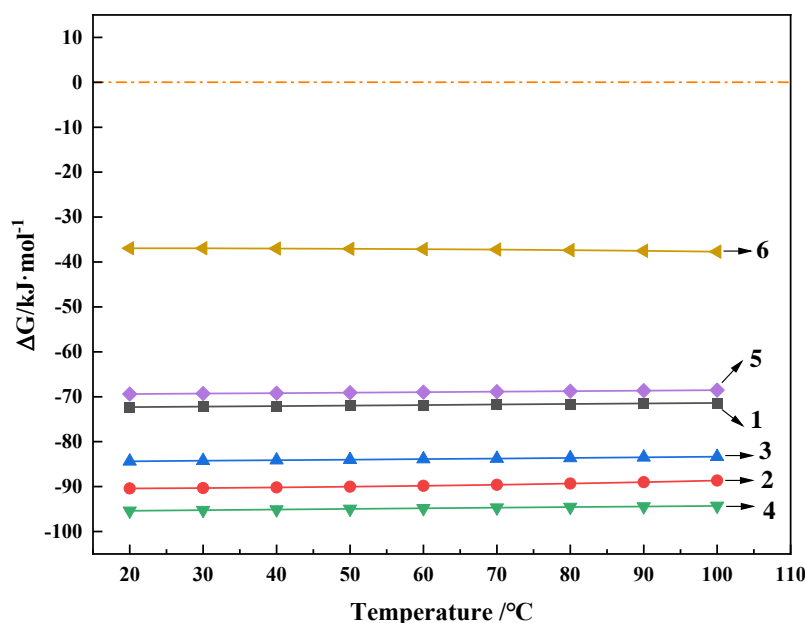


Fig. 2.  $\Delta G$  of reactions during the lime transforming of REMSES (20-100°C, the numbers correspond to the reaction numbers in Table 4)

### 3.2.1 Effect of lime dosage

The impact of lime dosage on the transformation process and leaching efficiencies of REEs and Li in REMSES was investigated at a lime/slag mass ratio ranging from 0 to 1.0, while keeping other parameters constant, including a transforming temperature of 90 °C and a transforming time of 120 min. The results are shown in Fig. 3.

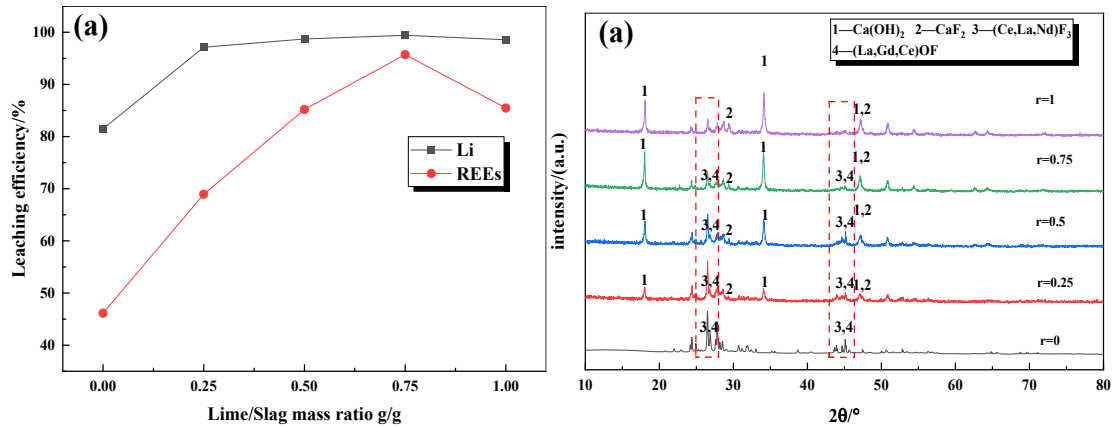


Fig. 3. (a) effect of lime dosage on leaching efficiencies of REEs and Li, (b) XRD patterns of transformed slag under different lime dosage

The results depicted in Fig. 3(a) demonstrate a gradual increase in the extraction of REEs and Li as lime dosage is increased. The leaching efficiencies for REEs increased from 46.14% to 95.72%, and for Li increased from 81.49% to 99.41%, as the lime/slag mass ratio increased from 0 to 0.75, followed by a slight decrease to 98.56% for Li and a decrease to 85.46% for REEs. The transformation of LiF was nearly complete at a lime/slag mass ratio of 0.25. In order to elucidate the disparity in leaching efficiency between rare earth elements (REEs) and lithium (Li), the correlation between temperature (T) and reaction free energy change ( $\Delta G$ ) was computed using HSC Chemistry software, as presented in Table 5, Table 6, and Fig. 4. The  $\Delta G$  values of the reactions between their respective fluorides and sulfuric acid suggest that LiF exhibits a higher extraction efficiency compared to REE<sub>3</sub> in the presence of sulfuric acid.

The increase in leaching efficiencies can be attributed to the disparity in  $\Delta G$  values when fluorides and hydroxides of REEs and Li react with sulfuric acid. The  $\Delta G$  values of reactions between fluorides and sulfuric acid are comparatively higher than those of hydroxides, suggesting that hydroxides exhibit greater ease of extraction in sulfuric acid.

Table 5.  $\Delta G$  of reactions between fluorides and sulfuric acid (20-100°C)

No.	Reaction	$\Delta_r G \sim T$ (kJ/mol)
7	$2LaF_3 + 3H_2SO_4 = La_2(SO_4)_3(a) + 6HF(g)$	$-0.6649T + 83.977$
8	$2CeF_3 + 3H_2SO_4 = Ce_2(SO_4)_3(a) + 6HF(g)$	$0.0588T + 50.8971$
9	$2PrF_3 + 3H_2SO_4 = Pr_2(SO_4)_3(a) + 6HF(g)$	$0.0756T + 47.484$
10	$2NdF_3 + 3H_2SO_4 = Nd_2(SO_4)_3(a) + 6HF(g)$	$-0.6057T + 209.82$
11	$2GdF_3 + 3H_2SO_4 = Gd_2(SO_4)_3(a) + 6HF(g)$	$0.0577T + 105.95$
12	$2LiF + H_2SO_4 = Li_2SO_4(a) + 2HF(g)$	$-0.1425T - 11.389$

Table 6.  $\Delta G$  of reactions between hydroxides and sulfuric acid (20-100°C)

The decrease in leaching efficiencies at a lime/slag mass ratio of 1.0 can be attributed to the formation of calcium sulphate due to an excessive amount of lime, which reacts with sulfuric acid and consequently reduces the concentration of acid in the liquid phase as well as the target metals (REEs and Li) in the solid phase. The main possible reaction equations during leaching process are listed as follows:

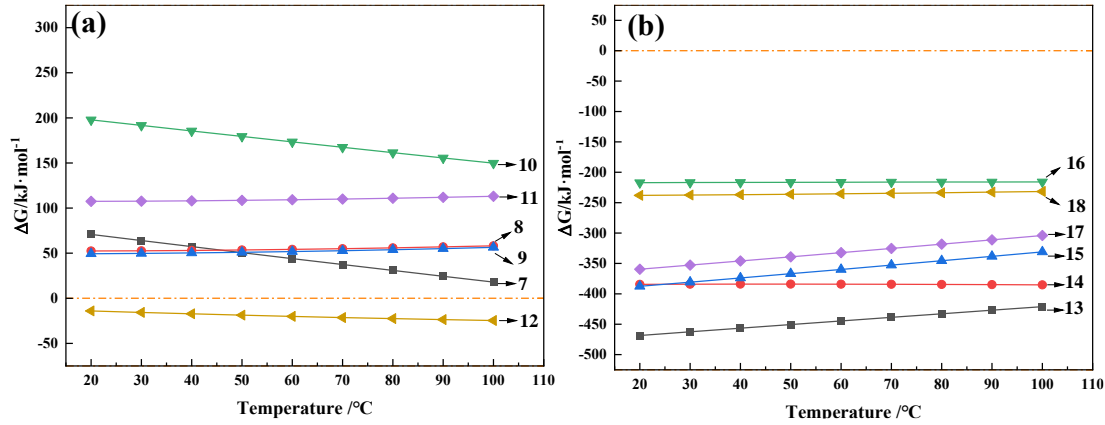
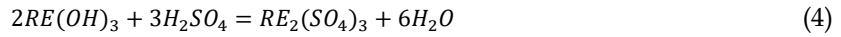


Fig. 4.  $\Delta G$  of reactions between fluorides(a)/hydroxides(b) and sulfuric acid (20-100°C).

The  $\Delta G$  value for reaction (7) was determined to be positive (17.46~21.44 kJ/mol at temperatures ranging from 20 to 100 °C) using HSC software, whereas the rest of the reactions exhibited negative values. Consequently, reaction (7) is deemed irrelevant. The XRD patterns of the transformed products at various lime dosages are depicted in Fig 3(b). It is evident that the peak intensity of REF3 decreases with an increasing proportion of lime dosage, indicating a transformation of REF3. Furthermore, it offers an explanation for the enhanced leaching efficiencies. The potential reactions occurring during lime transformation are enumerated based on the XRD analysis.



### 3.2.2. Effect of transforming temperature and time

The impact of varying temperature and duration on the leaching efficiencies of rare earth elements (REEs) and lithium from molten salt slag was investigated in Fig. 5, with ranges of 30 to 90 °C and 30 to 150 minutes respectively, while maintaining a fixed lime/slag mass ratio of 0.75. The results presented in Fig. 5(a) demonstrate a significant enhancement in the leaching efficiencies of REEs and Li as the temperature increased up to 60 °C, with remarkable improvements observed from 71.48% to 94.99% for REEs and from 98.12% to 99.42% for Li. The metal extractions tended to reach equilibrium when the temperature exceeded 60 °C. The extraction of REEs and Li increased with time until 120 min, as depicted in Fig. 5(b), resulting in enhanced leaching efficiencies from 62.90% to 95.05% for REEs and from 99.07% to 99.49% for Li. Upon further prolongation of the transformation time, there was a slight increase in metal extraction. Consequently, lime was employed to achieve equilibrium in the transformation of REEs and Li. After considering the correlation between energy consumption and overtemperature as well as prolonged transforming time, a transforming temperature of 60 °C and a transforming time of 120 min were selected to attain the highest leaching efficiency for both REEs and Li.

### 3.3 Effect of leaching conditions on rare earth and lithium leaching

The leaching conditions of transformed slag were conducted under various concentrations of sulfuric acid, L/S ratios, leaching temperatures, and durations while maintaining a fixed lime/slag mass ratio of 0.75, transforming temperature at 60 °C, and transforming time for 120 minutes. The investigation was conducted under fixed initial conditions, including a L/S ratio of 5, a leaching time of 120 minutes, and a leaching temperature of 90 °C.

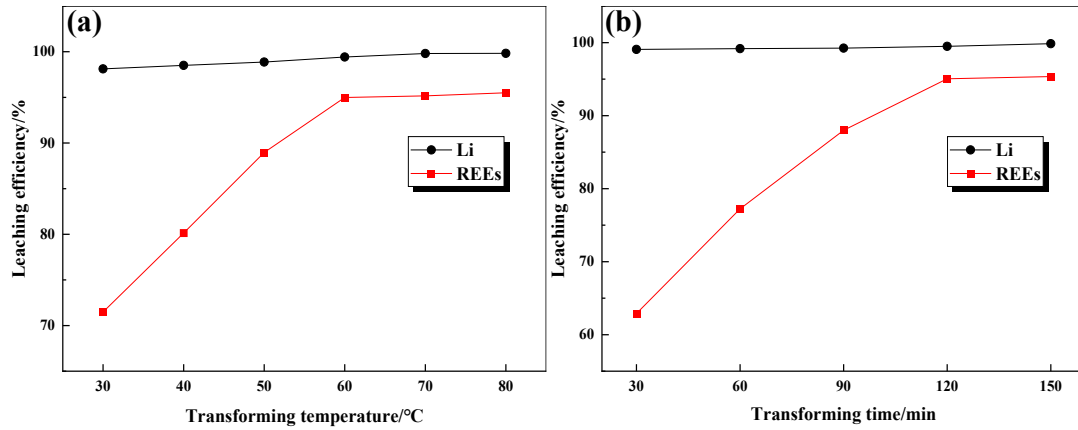


Fig. 5. Effect of (a) transforming temperature and (b) transforming time on leaching efficiency of REEs and Li

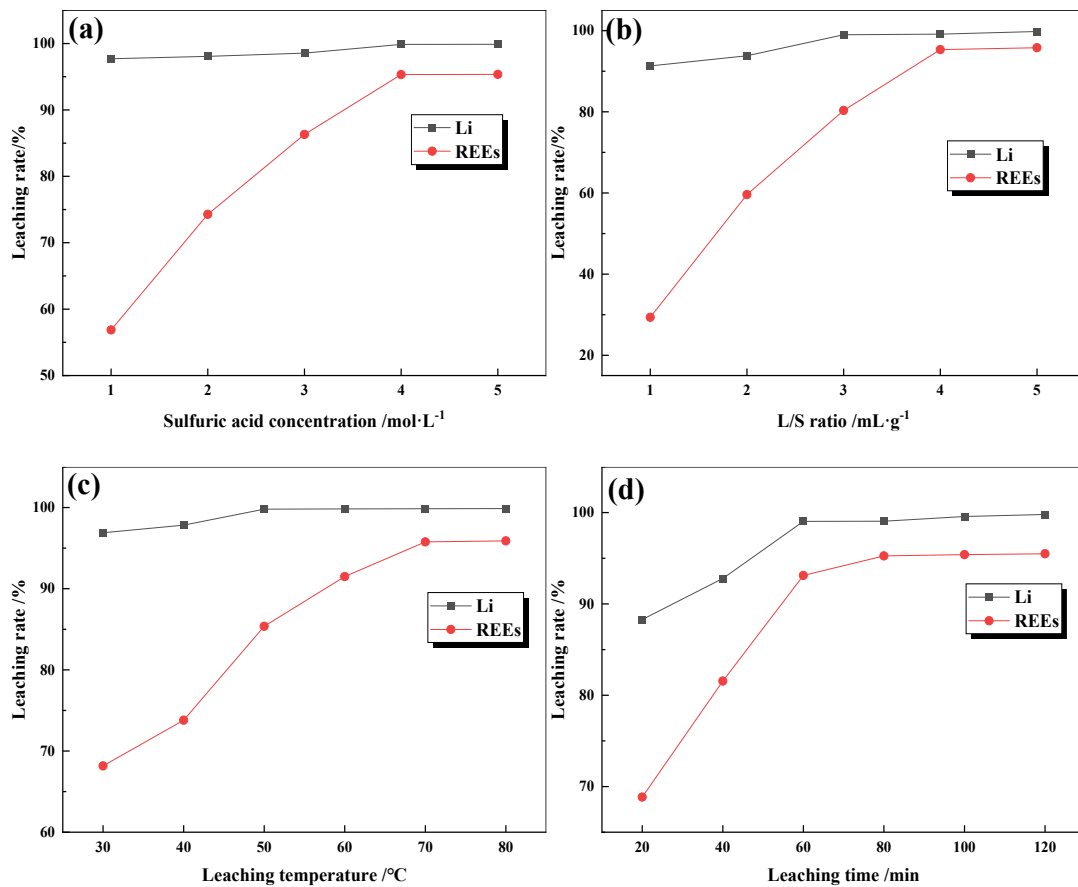


Fig. 6. Effect of leaching conditions on leaching efficiencies of REEs and Li : (a) Sulfuric acid concentration; (b) L/S ratio; (c) Leaching temperature (d) Leaching time

The impact of varying sulfuric acid concentrations was examined while keeping other parameters constant. The leaching efficiencies of REEs and Li, as shown in Fig. 6(a), exhibited a gradual increase with the rise in sulfuric acid concentration, reaching 56.87% to 95.32% for REEs and 97.71% to 99.87% for Li. The variation in the impact of sulfuric acid concentration on the leaching efficiencies of REEs and Li can be elucidated by considering the  $\Delta G$  of the reaction. The leaching of LiF was found to be more pronounced than that of REE3 in the sulfuric acid system without lime transformation, as indicated by the results presented in Table 5. The initial leaching efficiency of Li (86.49%) is significantly higher than that of REEs (46.14%), as illustrated in Fig. 3(a). The transformation of LiF was nearly complete when

the lime/molten salt slag mass ratio reached 0.25, surpassing that of REF3 and indicating a higher efficiency in extracting Li at lower acid concentration. The sulfuric acid concentration had a more pronounced impact on the leaching efficiency of REEs in the transformed REMSES, while the leaching efficiencies of Li exhibited minimal changes. The impact of varying L/S ratios from 1 to 5 was investigated. As seen in Fig. 6(b), the leaching efficiencies for REEs and Li increased significantly from 29.36% to 95.77% and from 91.29% to 99.78%, respectively, as the L/S ratio increased from 1 to 5. The impact of leaching temperature is investigated in Fig. 6(c). With an increase in the leaching temperature from 30 to 80 °C, the leaching efficiencies of rare earth elements (REEs) significantly increased from 68.17% to 95.89%, while the transformation efficiencies of lithium (Li) slightly improved from approximately 96.89% to 99.87%. The impact of leaching time on the leaching efficiency was examined, as illustrated in Fig. 6(d). The results revealed a significant increase in leaching efficiencies for REEs, from 68.85% to 93.12%, and for Li, from 88.29% to 99.04%, as the L/S ratio increased from 20 to 60 min. Subsequently, the efficiencies reached a plateau at 95.49% for REEs and 99.80% for Li. After considering both energy and acid consumption, the optimal leaching conditions for achieving maximum leaching efficiency of REEs and Li were determined as follows: a sulfuric acid concentration of 4 mol/L, an L/S ratio of 4, a leaching temperature of 70 °C, and a leaching time of 80 min.

### 3.4. Effect of REEs Precipitation

#### 3.4.1. Effect of precipitation conditions on precipitation efficiency of REEs and Li

After removing the majority of solids from the leachate, a solution with a pH of 0.2 containing 66.16 g/L (calculated in TREO) and 4.05 g/L lithium was ultimately obtained. The chemical components of the leachate are shown in Table 7. The leachate precipitation conditions were investigated under various  $\text{H}_2\text{C}_2\text{O}_4$ /REEs mole ratios, precipitation equilibrium pH levels, precipitation temperatures, and durations at fixed initial conditions with an  $\text{H}_2\text{C}_2\text{O}_4$ /REEs mole ratio of 4, a precipitation time of 120 minutes, a precipitation temperature of 30 °C, and a precipitation equilibrium pH value of 1.

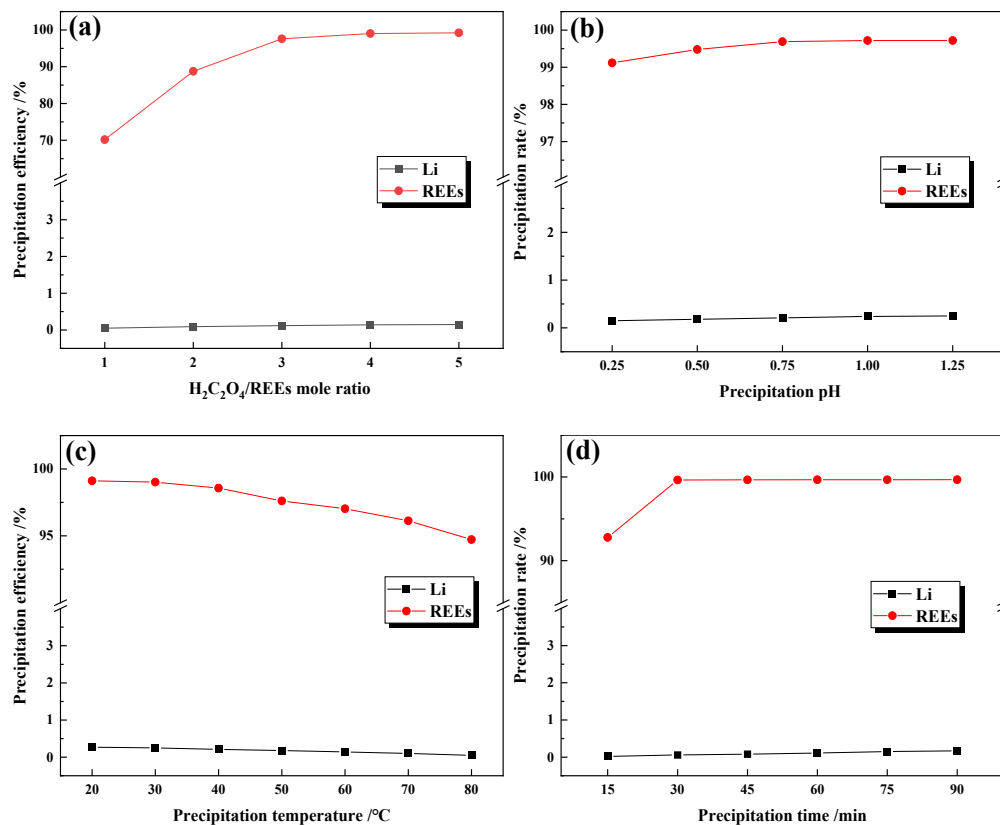


Fig. 7. Effect of precipitation conditions on precipitation efficiency of REEs and Li : (a)  $\text{H}_2\text{C}_2\text{O}_4$ /REEs mole ratio; (b) precipitation equilibrium pH; (c) precipitation temperature; (d) precipitation time

Table 7. Chemical components of the leachate (g/L)

TREO	Li	Fe	Mg	Al	pH*
66.16	4.05	10.18	3.32	3.85	0.21

\*Note: pH has no unit

Due to the exceptional selectivity of oxalic acid for REEs precipitation, the precipitation efficiencies of Li exhibit only minimal variation during the process of REEs precipitation, as depicted in Fig. 7. The precipitation efficiencies for the REEs increased from 70.18% to 99.21%, and for Li, they increased from 0.05% to 0.15%, as depicted in Fig. 7(a), with an increase in the  $\text{H}_2\text{C}_2\text{O}_4/\text{REEs}$  mole ratio from 1 to 5. The precipitation efficiency of both the REEs and Li slightly increased as depicted in Fig. 7(b) with the rise in equilibrium pH of precipitation. The obtained result suggests that the precipitation efficiency for the REEs and Li is minimally affected by the equilibrium pH of the solution. Consequently, adjusting the pH of the leachate for REEs precipitation can be disregarded. The obtained result suggests that the equilibrium pH of the solution exhibited minimal changes. Fig. 7(c) illustrates a decrease in both precipitation efficiency of REEs and Li with an increase in precipitation temperature. The increase in temperature led to an enhancement in the solubilities of the rare earth oxalates. The optimal precipitation temperature was determined to be 20 °C. As seen in Fig. 7(d), with increasing precipitation time, the precipitation efficiencies for the REEs increased from 92.78% to 99.68%, while the precipitation efficiencies for Li increased from 0.02% to 0.17%. The optimal precipitation conditions were determined as a  $\text{H}_2\text{C}_2\text{O}_4/\text{REEs}$  mole ratio of 4, a precipitation time of 30 minutes, and a precipitation temperature of 20°C, taking into account both energy efficiency and oxalic acid consumption.

### 3.4.2. Characterization of rare earth products

The precipitation of REEs has been successfully achieved with a precipitation efficiency of 99.68% and an overall recovery efficiency of 95.01%. After being separated from the liquid, the white crystals were washed and characterized then roasted at 900 °C for 2 hours to obtain REOs mixture. The XRD and SEM results for the white crystals and brown crystals are presented in Fig. 8 and Fig. 9, respectively. The diffraction peak observed in Fig. 9a for the white crystals exhibited a remarkable similarity to that of  $\text{RE}_2(\text{C}_2\text{O}_4)_3 \cdot 10\text{H}_2\text{O}$  ( $\text{Pr}_2(\text{C}_2\text{O}_4)_3 \cdot 10\text{H}_2\text{O}$ -Ref.00-018-1078,  $\text{Nd}_2(\text{C}_2\text{O}_4)_3 \cdot 10\text{H}_2\text{O}$ -Ref.00-018-0858  $\text{Gd}_2(\text{C}_2\text{O}_4)_3 \cdot 10\text{H}_2\text{O}$ -Ref. 00-020-0411). The diffraction peak of the brown crystals in Fig. 8a exhibited a striking resemblance to that of  $\text{RE}_2\text{O}_3$  (mixture of  $\text{CeO}_2$ -Ref. 00-034-0394,  $\text{Gd}_2\text{O}_3$ -Ref.00-012-0797,  $\text{NdPrO}_3$ -Ref.00-052-1438) indicating the high purity of  $\text{RE}_2\text{O}_3$ . Chemical analysis revealed that the purity of  $\text{RE}_2\text{O}_3$  was measured at 99.31%. The structure of  $\text{RE}_2\text{O}_3$ , as shown in Fig. 8b, exhibits excellent characteristics and renders it suitable for utilization as a raw material in the preparation of rare earth alloys.

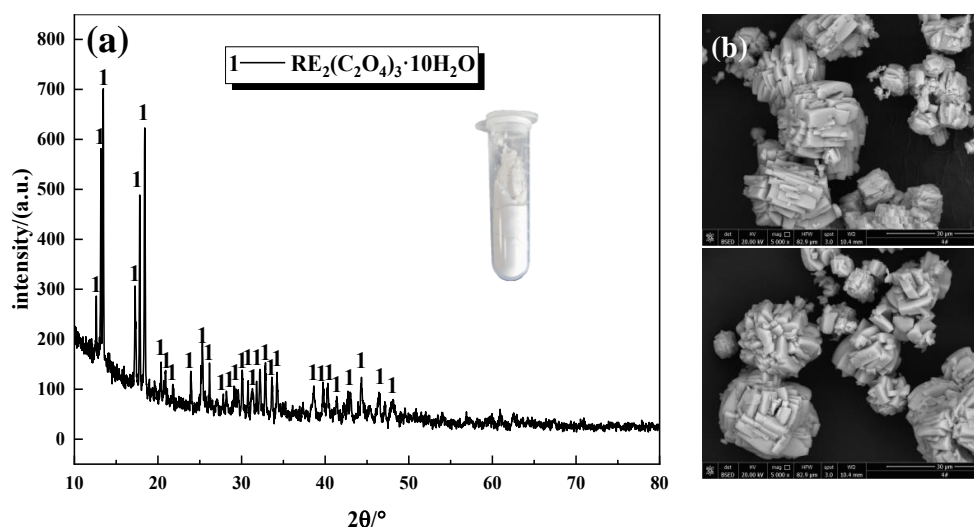
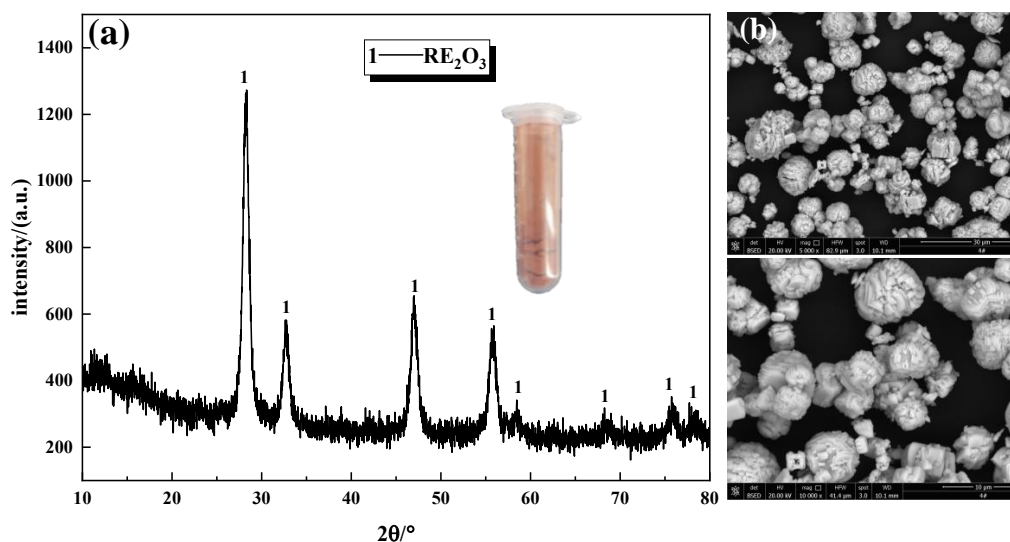


Fig. 8. XRD (a) and SEM (b) of the  $\text{RE}_2(\text{C}_2\text{O}_4)_3 \cdot 10\text{H}_2\text{O}$

Fig. 9. XRD (a) and SEM (b) of the RE<sub>2</sub>O<sub>3</sub>Table 8. Chemical composition of RE<sub>2</sub>O<sub>3</sub> (wt. %)

TREO	Ca	Fe	Al	Mg
99.31	0.05	0.02	0.02	0.02

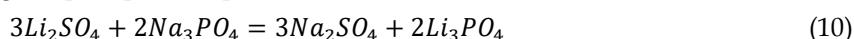
### 3.5. Preparation and characterization of the lithium phosphate product

The efficient precipitation of lithium phosphate can be achieved under conditions of low lithium concentration due to the low solubility product constant of lithium phosphate (Wang et al., 2018). Through experimental analysis, researches on the main chemical components of the liquid after rare earth precipitation were carried out, and the results are detailed in Table 9.

The results revealed a high concentration of lithium ions in the solution following the precipitation of rare earths. However, there remained numerous impurity ions, e.g. aluminum and iron ion. To achieve this objective, the experiment involved the addition of a saturated sodium hydroxide solution to the rare earth precipitation solution, gradually adjusting its pH to 9.0. Subsequently, a saturated sodium carbonate solution was added to further adjust the pH of the solution to 11.0. At this juncture, a substantial quantity of white precipitate emerged in the solution and was subsequently filtered to obtain a purified solution. The chemical composition analysis of the purified solution is presented in Table 9.

The results revealed a reduction in the lithium concentration in the purified solution from 3.98 g/L to 3.42 g/L, indicating a lithium loss rate of 13.72%. The simultaneous low concentration of aluminum and magnesium ions suggests that impurity content can be effectively reduced through alkali neutralization. Additionally, a sodium phosphate solution with a molar ratio of Na<sub>3</sub>PO<sub>4</sub>/Li of 1.1 was introduced into the purified solution, and subsequently subjected to chemical precipitation at a reaction temperature of 90°C for a duration of 1 hour. The resulting mixture was then filtered to obtain lithium phosphate products along with an accompanying post-precipitation solution.

The chemical composition of the liquid following lithium deposition is presented in Table 9. The results indicate a low lithium concentration of only 0.18g/L in the post-precipitation solution, with an impressive precipitation rate of 94.85% and an overall recovery rate of 80.75%. The primary chemical reactions that take place during the precipitation process of lithium are as follows:



The lithium phosphate products were subjected to XRD and SEM characterization, followed by chemical analysis. The obtained results are presented in Fig. 9 and Table 10, respectively. The results depicted in Fig. 10 demonstrate that the X-ray diffraction (XRD) patterns of lithium phosphate exclusively exhibit peaks corresponding to Li<sub>3</sub>PO<sub>4</sub> (Ref.00-015-0760), showcasing a well-defined

morphology. The results presented in Table 10 demonstrate that the lithium phosphate product exhibits a Li content of 17.79%, negligible levels of impurities, and a purity rating of 98.93%.

Table 9. Chemical components of the REEs precipitated solution (g/L)

Items	TREO	Li	Fe	Mg	Al	pH*
REEs precipitated solution	0.21	3.98	9.96	3.12	3.64	0.15
Purified solution	0.001	3.42	0.08	0.15	0.04	11.15
Lithium precipitated solution	0.001	0.18	0.01	0.01	0.01	12.27

\*Note: pH has no unit

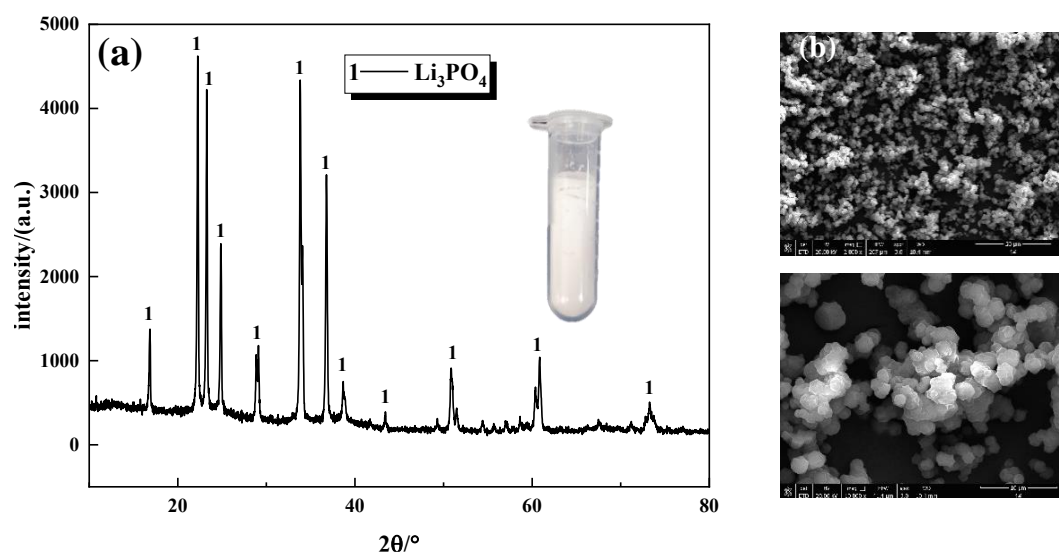


Fig. 10. XRD (a) and SEM (b) of the Lithium phosphate precipitation

Table 10. Chemical components of Lithium phosphate precipitate (wt. %).

Li	Ca	Mg	Fe	Al	Na	Si	SO <sub>4</sub> <sup>2-</sup>
17.79	0.11	0.15	0.05	0.05	0.10	0.02	0.40

### 3.6. Flowchart of recovery for rare earth and lithium from REMSES

Based on the investigation and discussion, a process flowchart for the recovery for REEs and lithium from REMSES by sulfuric acid leaching and selective precipitation is proposed in Fig. 11. In this flowchart, 95% of the REEs and 99% of the Li were leached under the optimal conditions. Then, 98.43% of the REEs were selectively precipitated, only 0.15% of Li was coprecipitated from the leachate by oxalic acid, and RE<sub>2</sub>(C<sub>2</sub>O<sub>4</sub>)<sub>3</sub>·10H<sub>2</sub>O with a purity of 99.31% was obtained. Finally, 94.85% of the Li was recovered by precipitation with sodium phosphate, and Li<sub>3</sub>PO<sub>4</sub> with a purity of 99.93% was obtained. Na<sub>3</sub>PO<sub>4</sub>·12H<sub>2</sub>O was recovered from the precipitated Li wastewater by evaporation crystallization, and the purified wastewater was reused for leaching. Through the above process, 95.01% of the REEs and 80.75% of the Li were recovered from REMSES. The process has the advantages of a high comprehensive utilization of resources and no secondary solid waste or wastewater pollution.

## 4. Conclusions

(1) A novel and simplified process was developed for efficient separating and coextracting rare earth elements (REEs) and lithium from REMSES. Compared to traditional methods used to recover REEs from electrolytic slag, this process ensures effective retrieval of REEs while comprehensively recovering available lithium, resulting in high resource utilization efficiency and cost-effective recovery.

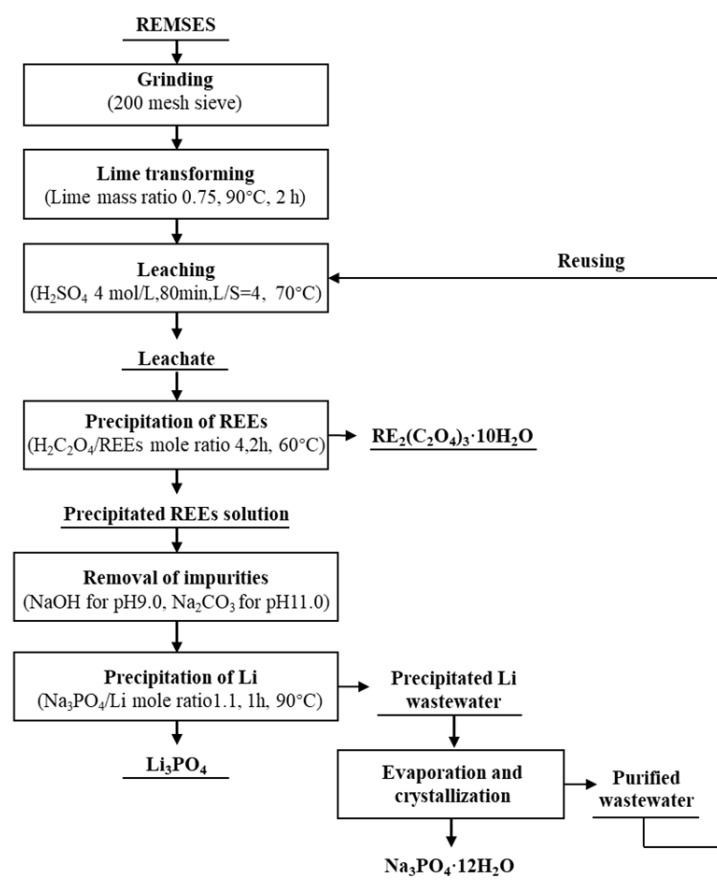


Fig. 11. Process flowchart of co-extracted REEs and Li from REMSES

- (2) The lime transformation is crucial for achieving the simultaneous extraction of REEs and lithium. The thermodynamic results demonstrate that rare earth fluorides can be readily transformed into rare earth hydroxides under the regulation of a strong alkali. The leaching rates of REEs and iron reach 95% and 98%, respectively, under the optimized lime transition and sulfuric acid leaching conditions, enabling simultaneous leaching of both elements.
- (3) The REEs and lithium were precipitated as  $\text{RE}_2(\text{C}_2\text{O}_4)_3 \cdot 10\text{H}_2\text{O}$  and  $\text{Li}_3\text{PO}_4$ , respectively, from the leachate after neutralization and removal of impurities. The rare earth precipitation resulted in the precipitation of 99.02% of REEs and 0.15% of lithium, yielding REOs with a purity of 99.31%. After the removal of impurities, lithium phosphate with a purity of 98.93% was precipitated during the lithium precipitation process, demonstrating an impressive lithium precipitation rate of 94.85% and an overall lithium recovery rate of 80.75%.

### Acknowledgements

This work was supported by the Open Project for Key Laboratory of Testing and Tracing of Rare Earth Products for State Market Regulation, Jiangxi University of Science and Technology (No. TTREP2022ZD01 and TTREP2022YB02).

### References

- CAI, B., LIU, H., KOU, F., YANG, Y., YAO, B., CHEN, X., WONG, D., ZHANG, L., LI, J., KUANG, G., 2018. Estimating perfluorocarbon emission factors for industrial rare earth metal electrolysis. *Resour Conserv Recy.* 136, 315-323.
- CHEN, J., SUN, S., TU, G., & XIAO, F., 2023. Review of efficient recycling and resource utilization for rare earth molten salt electrolytic slag. *Miner Eng.* 204, 108425.
- CHEN, L., XU, J., YU, X., TIAN, L., WANG, R., XU, Z., 2021. Thermodynamics and Kinetics of Sulfuric Acid Leaching Transformation of Rare Earth Fluoride Molten Salt Electrolysis Slag. *Front Chem.* 9, 574722.

- CHEN, X., SUN Y., WANG, L., QU, X., ZHAO, Y., XIE, H., WANG, D., YIN, H., 2023. *Electrochemically recycling degraded superalloy and valorizing CO<sub>2</sub> in the affordable borate-modified molten electrolyte*. Tungsten. 1-12.
- DUAN, W., WANG, Y., LI, R., REN, Z., ZHOU, Z., 2024. *Selective extraction of lithium from high magnesium/lithium ratio brines with a TBP-FeCl<sub>3</sub>-P204-kerosene extraction system*. Sep Purif. Technol. 328, 125066.
- DUSHYANTHA, N., BATAPOLA, N., ILANKOON, I. M. S. K., ROHITHA, S., PREMASIRI, R., ABEYSINGHE, B., RATNAYAKE, NALIN., DISSANAYAKE, K., 2020. *The story of rare earth elements (REEs): Occurrences, global distribution, genesis, geology, mineralogy and global production*. Ore Geol Rev. 122, 103521.
- FENG, B., ZHAO, Z., JIA, Y., AN, J., WANG, M., 2023. *Optimal V<sub>2</sub>O<sub>3</sub> extraction by sustainable vanadate electrolysis in molten salts*. Tungsten. 1-9.
- General Administration of Quality Supervision, Inspection and Quarantine of the People's Republic of China, Standardization Administration of the People's Republic of China. 2020. *Rare earth metals and their compounds – Determination of total rare earth content*. (GB/T 14635-2020).
- GEORGIOS C., KONSTANTINOS I. V., BAKLAVARIDIS A., BENETIS P., 2015. *Rare Earth Elements: Industrial Applications and Economic Dependency of Europe*. Procedia Comput. Sci. 24, 126-135.
- GU, Y., LIU, J., QU, S., DENG, Y., HAN, X., HU, W., ZHONG, C., 2017. *Electrodeposition of alloys and compounds from high-temperature molten salts*. J. Alloy Compd. 690, 228-238.
- HU, H., WANG, J., 2021. *Selective extraction of rare earths and lithium from rare earth fluoride molten-salt electrolytic slag by nitration*. Hydrometallurgy. 200: 105552.
- JI, B., LI, Q., ZHANG, W., 2022. *Leaching recovery of rare earth elements from the calcination product of a coal coarse refuse using organic acids*. J. Rare Earth. 40(02), 318-327.
- LAI, Y., LI, J., ZHU, S., LIU, K., XIA, Q., HUANG, M., HU, G., ZHANG, H., QI, T., 2023. *Recovery of rare earths, lithium, and fluorine from rare earth molten salt electrolytic slag by mineral phase reconstruction combined with vacuum distillation*. Sep Purif Technol. 310, 123105.
- LI, M., LIU, Z., WU, J., HU, Y., 2009. *Element and analytical Chemistry of earth elements*, Chemical Industry Press.
- LIANG, Y., LI, Y., XUE, L., ZOU, Y., 2018. *Extraction of rare earth elements from fluoride molten salt electrolytic slag by mineral phase reconstruction*. J. Clean Prod. 177(3), 567-572.
- LIU, H., AZIMI, G., 2021. *Process analysis and study of factors affecting the lithium carbonate crystallization from sulfate media during lithium extraction*. Hydrometallurgy. 199, 105532.
- LIU, Y., GAO, F., CHEN, T., WANG, C., HU, K., ZHANG, C., HUANG, Z., LI, X., WAN, Y., 2023. *Effective recovery of rare earth and fluorine from REF3 smelting slag by a mechanochemical process*. Sep Purif Technol. 316, 123832.
- LIU, Z., ZHOU, H., LI, W., LUO, X., WANG, J., LIU, F., 2022. *Separation and coextraction of REEs and Fe from NdFeB sludge by co-leaching and stepwise precipitation*. Sep Purif. Technol. 282, 119795.
- MULWANDA, J., SENANAYAKE, G., OSKIERSKI, H. C., ALTARAWNEH, M., DLUGOGORSKI, B. Z., 2023. *Extraction of lithium from lepidolite by sodium bisulphate roasting, water leaching and precipitation as lithium phosphate from purified leach liquors*. Hydrometallurgy. 222, 106139.
- Outokumpu Technology Company, 2012. *HSC Chemistry 6.0 software*.
- PRINCE, S., AVIMANYU D., COURTNEY Y., 2021. *Extraction and optimization of neodymium from molten fluoride electrolysis*. Separation and Purification Technology. 256, 117770.
- SU, J., XU, R.; NI, S., LI, F., SUN, X., 2020. *A cost-effective process for recovering thorium and rare earths from radioactive residues*. J. Cleaner Prod. 254, 119931.
- SUN, H., WANG, T., LI, C., YANG, Y., 2022. *Recycling rare earth from ultrafine NdFeB waste by capturing fluorine ions in wastewater and preparing them into nano-scale neodymium oxyfluoride*. J. Rare Earth. 40(5), 815-821.
- TIAN, L., CHEN, L., GONG, A., WU, X., CAO, C., XU, Z., 2021. *Recovery of rare earths, lithium and fluorine from rare earth molten salt electrolytic slag via fluoride sulfate conversion and mineral phase reconstruction*. Minerals Engineering. 70, 106965.
- TONG Z., HU X., WEN H., 2022. *Effect of roasting activation of rare earth molten salt slag on extraction of rare earth, lithium and fluorine*. J. Rare Earth. 41(2), 300-308.
- WANG, J., CUI J., WANG, X., QIN, X. *Inorganic chemistry*. Higher Education Press, 2018.
- WANG, J., HU, H., 2021. *Selective extraction of rare earths and lithium from rare earth fluoride molten-salt electrolytic slag by sulfation*. Miner Eng. 160, 106711.
- WU, H., YAN, H., LIANG, Y., QIU, S., ZHOU, X., ZHU, D., QIU, T., 2023. *Rare earth recovery from fluoride molten-salt electrolytic slag by sodium carbonate roasting-hydrochloric acid leaching*. J. Rare Earths. 41(8), 1242-1249.

- WU, L., ZHANG, J., HUANG, Z., ZHANG, Y., XIE, F., ZHANG, S., FAN, H., 2023. *Extraction of lithium as lithium phosphate from bauxite mine tailings via mixed acid leaching and chemical precipitation*. *Ore Geol Rev.* 105621.
- XING P., LI, H., YE, C., ZHONG, L., 2022. *Recovery of Rare-Earth Elements from Molten Salt Electrolytic Slag by Fluorine Fixation Roasting and Leaching*. *J Sustain Metall.* 8(1),522-531.
- YANG, D., YU, M., MUBULA, Y., YUAN, W., HUANG, Z., LIN, B., MEI, G., QIU, T., 2023. *Recovering rare earths, lithium and fluorine from rare earth molten salt electrolytic slag using sub-molten salt method*. *J. Rare Earth.* 1002-0721.
- YANG, Y., LI, L., XIAO, M., NIU, F., 2019. *Transformation mechanism and leaching performance of rare earth fluoride molten salt slag in the process of Na<sub>2</sub>CO<sub>3</sub>-roasting*. *J. Central South Univ.(Science and Technology).* 50(5), 1035-1041.
- YANG, Y., WEI, T., XIAO, M., NIU, F., SHEN, L., 2020. *Rare earth recovery from fluoride molten-salt electrolytic slag by borax roasting-hydrochloric acid leaching*. *JOM.* 72, 939-945.
- YANG, Z., XIAO, F., SUN, S., ZHONG, H., TU, G., 2023. *REEs recovery from molten salt electrolytic slag: Challenges and opportunities for environmentally friendly techniques*. *Journal of Rare Earths.* 1002-0721.